Gigahertz photon density waves in a turbid medium: Theory and experiments

Joshua B. Fishkin,[1,*] Sergio Fantini,[1] Martin J. vandeVen,[2] and Enrico Gratton[1]
[1]*Laboratory for Fluorescence Dynamics, Department of Physics, University of Illinois at Urbana-Champaign, 1110 West Green Street, Urbana, Illinois 61801*
[2]*ISS Inc., 2604 North Mattis Avenue, Champaign, Illinois 61821*
(Received 4 August 1995)

The predictions of the frequency-domain standard diffusion equation (SDE) model for light propagation in an infinite turbid medium diverge from the more complete P_1 *approximation* to the linear Boltzmann transport equation at intensity modulation frequencies greater than several hundred MHz. The P_1 *approximation* is based on keeping only the terms $l=0$ and $l=1$ in the expansion of the angular photon density in spherical harmonics, and the nomenclature P_1 *approximation* is used since the spherical harmonics of order $l=1$ can be written in terms of the first order Legendre polynomial, which is traditionally represented by the symbol P_1. Frequency-domain data acquired in a quasi-infinite turbid medium at modulation frequencies ranging from 0.38 to 3.2 GHz using a superheterodyning microwave detection system were analyzed using expressions derived from both the P_1 aproximation equation and the SDE. This analysis shows that the P_1 approximation provides a more accurate description of the data over this range of modulation frequencies. Some researchers have claimed that the P_1 approximation predicts that a light pulse should propagate with an average speed of $c/\sqrt{3}$ in a thick turbid medium. However, an examination of the Green's function that we obtained from the frequency-domain P_1 approximation model indicates that a photon density wave phase velocity of $c/\sqrt{3}$ is only asymptotically approached in a regime where the light intensity modulation frequency aproaches infinity. The Fourier transform of this frequency-domain result shows that in the time domain, the P_1 approximation predicts that only the leading edge of the pulse (i.e., the photons arriving at the detector at the earliest time) approaches a speed of $c/\sqrt{3}$.

PACS number(s): 05.60.+w

I. INTRODUCTION

Frequency-domain methods, in which the light source intensity is modulated at radio frequency, have been successfully applied to spectroscopy studies of turbid media [1–4]. In macroscopically homogeneous media, simple expressions for the absorption and reduced scattering coefficients were obtained in the strongly scattering regime, where the photon mean-free path is much shorter than the source-detector separation [5,6]. These expressions are based on the standard diffusion equation (SDE), which is valid when the photon current density **J** is related to the photon density U by Fick's law [7,8]. This condition is satisfied in turbid media with relatively large scattering coefficients and at modulation frequencies up to hundreds of MHz. The refraction and diffraction of the diffuse photon density waves predicted by the SDE has been experimentally studied [9,10]. At GHz modulation frequencies, the SDE is expected to break down [11,12]. In this paper we study this GHz frequency region theoretically and experimentally. Theoretically, we have conducted a comparison between the SDE and the more complete P_1 approximation to the Boltzmann transport equation. The P_1 approximation is based on keeping only the terms $l=0$ and $l=1$ in the expansion of the angular photon density in spherical harmonics, and the nomenclature P_1 *approximation* is used since the spherical harmonics of order $l=1$ can be written in terms of the first order Legendre polynomial, which is traditionally represented by the symbol P_1. Expansion of the angular photon density in terms of the first $L+1$ spherical harmonics is generally referred to as a P_L approximation [7]. Experimentally, we have employed a frequency down-conversion technique. This technique extends the useful bandwidth of our microchannel plate detector to about 4 GHz.

In the application of frequency-domain methods to the optical study of biological tissue, there are a number of reasons for considering the use of modulation frequencies in the GHz region. In spectroscopy, intrinsic tissue inhomogeneities can affect the intensity and the phase shift measurement to different extents. In fact, the influence of the optical properties of a specific spatial region can be substantially different in the intensity and phase measurements [13]. The use of only one parameter, be it the intensity, the demodulation, or the phase shift information, might thus be preferable due to instrument configuration considerations. To be effective in recovering the tissue optical parameters, though, measurements in a modulation frequency range extending from a few MHz up to a

*Present address: Beckman Laser Institute and Medical Clinic, University of California at Irvine, 1002 Health Sciences Road East, Irvine, CA 92715.

few GHz may be required. In this paper we discuss the range of optical parameters that can be recovered from the measurement of a single quantity, i.e., the phase of the photon density wave in a range of modulation frequencies. Another reason for doing measurements at GHz modulation frequencies is to perform localized tissue spectroscopy. The use of higher modulation frequencies reduces the probed volume of tissue [12,14]. In imaging, it has been shown that measurements at higher modulation frequencies provide better resolution than measurements at lower modulation frequencies [14–16].

In this work, we also discuss the limiting phase velocity of the photon density wave predicted by the frequency-domain solution of the P_1 approximation to the Boltzmann transport equation. We describe how this limiting phase velocity relates to the leading edge of pulse propagation in a turbid medium.

II. THEORY

A. P_1 approximation to the Boltzmann transport equation

A first order spherical harmonics expansion of the angular photon density (i.e., the radiance) in the Boltzmann transport equation yields the P_1 approximation equation [7,8]

$$cD\left[\frac{3}{c^2}\frac{\partial^2 U(\mathbf{r},t)}{\partial t^2}-\nabla^2 U(\mathbf{r},t)\right]+(1+3\mu_a D)\frac{\partial U(\mathbf{r},t)}{\partial t}+c\mu_a U(\mathbf{r},t)=S^{(0)}(\mathbf{r},t)\ , \quad (1)$$

with

$$S^{(0)}(\mathbf{r},t)\equiv q_0(\mathbf{r},t)+\frac{3D}{c}\frac{\partial q_0(\mathbf{r},t)}{\partial t}-3D\nabla\cdot q_1(\mathbf{r},t)\ .$$

$U(\mathbf{r},t)$ is the density of photons (with units of photons/volume), $\mathbf{r}$ is position, t is time, c is the speed of a photon in the transporting medium (i.e., water in our experiments),

$$D\equiv\frac{1}{3(\mu_a+\mu_s')} \quad (2)$$

is the diffusion coefficient (with units of distance),

$$\mu_s'\equiv(1-g)\mu_s \quad (3)$$

is the reduced scattering coefficient (with units of inverse distance), g is the average of the cosine of the scattering angle after a photon collision, and μ_a and μ_s, respectively, are the inverse of the mean-free path for photon absorption and the inverse of the mean-free path for elastic scattering collisions (μ_a and μ_s have units of inverse distance). $S^{(0)}(\mathbf{r},t)$ is the photon source, with $q_0(\mathbf{r},t)$ being the isotropic term in a first-order spherical harmonics expansion of the source term in the Boltzmann transport equation, and $\mathbf{q}_1(\mathbf{r},t)$ is the first moment in this expansion which describes the dipole-like anisotropy of the source. Equation (1) reasonably approximates the Boltzmann transport equation when $\mathbf{r}$ is far from sources and boundaries, and $\mu_s/(\mu_a+\mu_s)$ is close to unity, i.e., $\mu_s \gg \mu_a$ [7,8].

In the frequency domain, the source term $S^{(0)}(\mathbf{r},t)$ in Eq. (1) is given by

$$S^{(0)}(\mathbf{r},t)=\delta(\mathbf{r})S\{1+A\exp[i(\omega t+\varepsilon)]\}\ , \quad (4)$$

where $\delta(\mathbf{r})$ is a three-dimensional Dirac delta function located at the origin, S is the source strength (in photons per second). A is the modulation of the source, $i=\sqrt{-1}$, ω is the angular modulation frequency of the source, and ε is an arbitrary phase. The assumption that $1\gg 3\mu_a D\gg(3\omega D/c)^2$ reduces the P_1 approximation equation [i.e., Eq. (1)] to the standard diffusion equation (SDE)

$$\frac{\partial U(\mathbf{r},t)}{\partial t}+c\mu_a U(\mathbf{r},t)-cD\nabla^2 U(\mathbf{r},t)=S^{(0)}(\mathbf{r},t)\ , \quad (5)$$

with $S^{(0)}(\mathbf{r},t)$ given in Eq. (4).

Using Eq. (2) and the above mentioned assumption that $1\gg 3\mu_a D$ (which means that $\mu_s'\gg\mu_a$), we write

$$\frac{3\omega D}{c}=\frac{\omega}{c(\mu_a+\mu_s')}\cong\frac{\omega}{c\mu_s'} \quad (6)$$

(Neglect of μ_a in the diffusion coefficient D in the SDE approximation has been previously noted by Furutsu and Yamada) [17]. We have now reached a critical point in our discussion. In the P_1 approximation to the Boltzmann transport equation as represented by Eq. (1), the assumption is that $\mu_s\gg\mu_a$. Since a condition for the validity of the SDE is $1\gg 3\mu_a D$, the further assumption that $\mu_s'\gg\mu_a$ is necessary in order to reduce the P_1 approximation equation to the SDE, as represented by Eq. (5). The P_1 approximation equation thus involves an assumption about the scattering coefficient μ_s, whereas the SDE involves an additional assumption about the reduced scattering coefficient μ_s'. μ_s' is typically an order of magnitude less than μ_s in biological tissue, since g is of the order of 0.9 [18]. In these conditions of highly forward scattering ($g=0.9$), Fig. 1(a) shows the regions of the $\mu_s'-\mu_a$ plane where one can apply the P_1 approximation and the SDE. In Fig. 1(a), the conditions of applicability of P_1 and SDE ($\mu_s\gg\mu_a$ and $\mu_s'\gg\mu_a$, respectively) are written $\mu_s>10\mu_a$ and $\mu_s'>10\mu_a$, respectively. The choice of the factor 10 is arbitrary, so that Fig. 1(a) should not be interpreted rigorously. Nevertheless, it gives an idea of the values of the optical coefficients μ_a and μ_s' for which the P_1 and SDE approximations to the Boltzmann transport equation (BTE) are applicable. We observe that in the case of isotropic scattering ($g=0$), the regions of the $\mu_s'-\mu_a$ plane where P_1 and SDE are applicable coincide. The other condition for the validity of the SDE, namely $1\gg 3\omega D/c$, requires that the modulation frequency $\omega/2\pi$ be much smaller than the effective scattering rate $c(\mu_a+\mu_s')$ divided by 2π. This condition is shown in Fig. 1(b), where we plot the product $r\mu_s'$ as a function of $r\omega/2\pi$. The condition for the validity of the SDE (i.e., $1\gg 3\omega D/c$) is written $\frac{1}{10}>3\omega D/c$ in Fig. 1(b). The reason for having $r\mu_s'$ on the y axis of Fig. 1(b) is that we can thus plot (using a single line) the condition $r\gg 1/\mu_s$ for the validity of the P_1 approximation. This condition (written as $r\mu_s>10$ or $r\mu_s'>1$ by considering

again $g=0.9$) limits the applicability of the P_1 approximation to the region above the line $r\mu_s'=1$ in Fig. 1(b). We will discuss this condition for the validity of the P_1 approximation below. Here we stress again that the factor 10 used to plot the conditions $\frac{1}{10}>3\omega D/c$ and $r\mu_s>10$ is an arbitrary factor used to interpret the actual conditions $1\gg 3\omega D/c$ and $r\mu_s\gg 1$, respectively. For this reason, Fig. 1(b) should not be taken as a rigorous representation of the limits of validity of P_1 and the SDE. We finally point out that one can use the SDE (P_1) approximation to describe adequately the experimental data in a given configuration only if such a configuration satisfies the requirements of both Figs. 1(a) and 1(b) for the SDE (P_1). In other words, given r, μ_a, μ_s', and $\omega/2\pi$, the corresponding points in Figs. 1(a) and 1(b) should both be in the SDE (P_1) region, to enable one to adequately apply the SDE (P_1) approximation. For example, Figs. 1(a) and 1(b) may give us an idea about the limit of applicability of the SDE in biological tissue. The values $\mu_a\sim 0.01-0.1$ cm^{-1} and $\mu_s'\sim 1-10$ cm^{-1}, which are typical of soft tissue, are certainly in the SDE region of Fig. 1(a). Figure 1(b) tells us that the P_1 approximation is applicable for source-detector separations down to about a few mm (or about 1 cm if we consider that g can be as small as 0.6 in tissues [18]), and the SDE is applicable for modulation frequencies up to about 1 GHz.

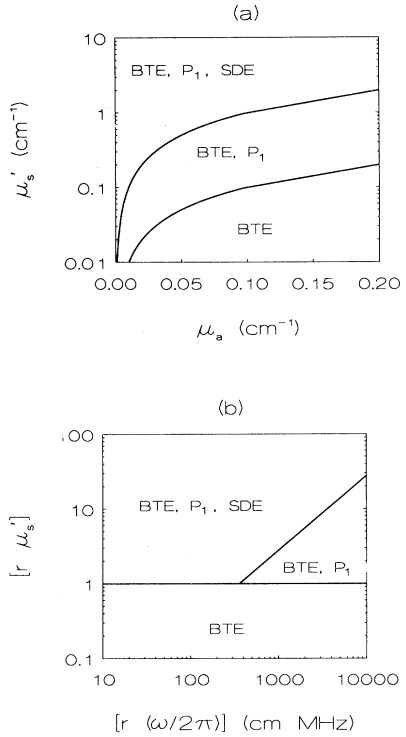

FIG. 1. Regions of applicability of the standard diffusion equation (SDE) and of the P_1 approximation to the Boltzmann transport equation (BTE). In these figures, g is assumed to be 0.9, so that $\mu_s=10\mu_s'$. (a) μ_s'-μ_a plane. The plotted conditions are $\mu_s'>\mu_a$ (for P_1), and $\mu_s'>10\mu_a$ (for SDE). (b) $r\mu_s'$-$r\omega/2\pi$ plane. The plotted conditions are $r\mu_s'>1$ (for P_1), and $1/10>3\omega D/c$ (for SDE).

B. Limiting value of the phase velocity

The first two terms in Eq. (1) have the form of a wave equation, and the first term in Eq. (1) has led to claims that the P_1 approximation equation predicts that a light pulse in a turbid medium propagates with an average speed of $c/\sqrt{3}$, c being the speed of a photon in the medium surrounding the scattering particles [19–21]. We shall now examine the validity of this claim by studying both the frequency and time-domain Green's function solutions of Eq. (1).

The infinite medium frequency-domain Green's function solution to Eq. (1) is

$$U_G(\mathbf{r},t)=\frac{1}{4\pi cDr}\exp\left[-r\left[\frac{\mu_a}{D}\right]^{1/2}\right]+\frac{1}{4\pi cDr}\exp[-rk\cos\theta+i(rk\sin\theta-\omega t-\varepsilon)]\,, \quad (7)$$

where k and θ are given by

$$k\equiv\left[\frac{(c\mu_a-\omega\alpha)^2+(\omega+c\mu_a\alpha)^2}{c^2D^2}\right]^{1/4}, \quad (8)$$

$$\theta\equiv\tfrac{1}{2}\tan^{-1}\left[\frac{\omega+c\mu_a\alpha}{c\mu_a-\omega\alpha}\right], \quad (9)$$

with

$$\alpha\equiv\frac{3\omega D}{c}\,. \quad (10)$$

In the limit in which the terms containing α are negligible, Eq. (7) reduces to the infinite medium frequency-domain solution given by Fishkin and Gratton for the SDE [Eq. (5)] [14]. Equation (7) yields expressions for the frequency-domain quantities measured at r relative to the corresponding quantities measured at r_0, namely, the steady-state photon density (dc), the amplitude of the photon density oscillations (ac), and the phase shift of the photon density wave (Φ). The relative quantities are given by

$$U_{\rm rel}^{\rm dc}\equiv\frac{U^{\rm dc}(r)}{U^{\rm dc}(r_0)}=\frac{r_0}{r}\exp\left[-(r-r_0)\left[\frac{\mu_a}{D}\right]^{1/2}\right], \quad (11)$$

$$U_{\rm rel}^{\rm ac}\equiv\frac{U^{\rm ac}(r)}{U^{\rm ac}(r_0)}=\frac{r_0}{r}\exp[-(r-r_0)k\cos\theta]\,, \quad (12)$$

$$\Phi_{\rm rel}\equiv\Phi(r)-\Phi(r)=(r-r_0)k\sin\theta\,. \quad (13)$$

The relative demodulation of the photon density wave is given by

$$M_{\rm rel}\equiv U_{\rm rel}^{\rm ac}/U_{\rm rel}^{\rm dc}\,. \quad (14)$$

The phase velocity V_p of a photon density wave in the P_1 approximation may be derived from Eq. (7):

$$V_p = \frac{\omega}{k \sin\theta} . \tag{15}$$

The ratio $V_p/(c/\sqrt{3})$ is plotted versus modulation frequency in Fig. 2, where V_p is given by Eq. (15), $c = 2.26 \times 10^{10}$ cm/s (the speed of light in water), $\mu_s' = 4.30$ cm^{-1}, and $\mu_a = 0.008$ cm^{-1}. One can see from Fig. 2 that the ratio $V_p/(c/\sqrt{3})$ asymptotically approaches 1 as the modulation frequency approaches infinity. Since a light pulse consists of a Fourier spectrum of photon density waves of different phase velocities and amplitudes, this result demonstrates that all of the Fourier components of a light pulse in this medium propagate at a speed that is slower than $c/\sqrt{3}$, according to the predictions of the P_1 approximation equation [Eq. (1)]. To further illustrate this point, we have plotted the time-domain Green's function solution to Eq. (1) in Fig. 3 using the same optical parameters used in Fig. 2. We obtained the time-domain plots of the photon density Green's function by numerically performing a Fourier transform of the frequency-dependent part of Eq. (7) using the commercial package MATHEMATICA (Wolfram Research, Inc., Champaign, IL). The results are shown in Fig. 3. Kaltenbach and Kaschke obtained an analytical Green's function solution in the time domain to the P_1 approximation equation (i.e., they obtained an analytical solution to Eq. (1) with the source term $S^{(0)}(\mathbf{r},t) = \delta(\mathbf{r})\delta(t)$ [22]. Time-domain results obtained when we numerically Fourier transformed the frequency-dependent part of Eq. (7) are identical to the results that Kaltenbach and Kaschke calculated directly from their analytical time-domain Green's function. Examination of these time-domain results shows that at a distance r from the light source, the earliest arriving photons arrive at a time $t_{\min} = r/(c/\sqrt{3})$. For the distance $r = 1.8$ cm and $c = 2.26 \times 10^{10}$ cm/s used in our Fig. 3 calculations, the time given by $r/(c/\sqrt{3})$ is 138 ps. This

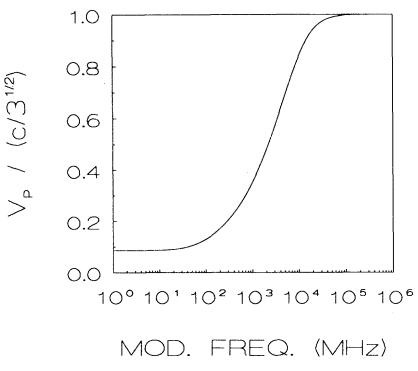

FIG. 2. The ratio $V_p/(c/\sqrt{3})$ vs modulation frequency. $c = 2.26 \times 10^{10}$ cm/s, i.e., c is the speed of light in water, $\mu_s' = 4.30$ cm^{-1}, and $\mu_a = 0.008$ cm^{-1}. V_p is calculated from Eq. (15).

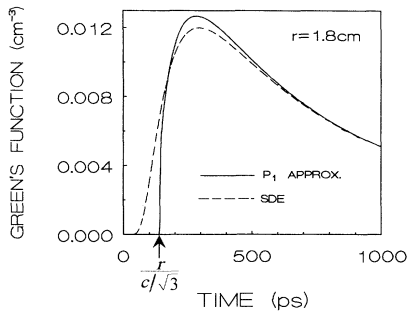

FIG. 3. Time-domain photon density Green's functions. $r = 1.8$ cm, $c = 2.26 \times 10^{10}$ cm/s, $\mu_s' = 4.30$ cm^{-1}, and $\mu_a = 0.008$ cm^{-1}. The plots were obtained by taking the Fourier transform of the frequency-domain photon density Green's functions [i.e., the frequency-dependent part of Eq. (7)]. The SDE plot was calculated with the assumption that the α terms in Eq. (7) were negligible.

is precisely the point on the time axis of Fig. 3 that the plot of the photon density impulse response function becomes nonzero.

Zaccanti *et al.* performed time-domain measurements of light pulse propagation in turbid media with optical parameters comparable to those given in Fig. 3 of this work [23]. They have compared their experimental results to the predictions of the SDE, and have stated in the conclusion of their paper that "the shapes of the pulses obtained with the diffusion approximation are similar to the measured pulses but significantly wider" [23]. Note that in Fig. 3 of our paper the pulse shape predicted by the SDE is considerably broader than the pulse shape predicted by the P_1 equation. This result indicates that the P_1 equation may provide a better description than the SDE of the pulse propagation data presented by Zaccanti *et al.*

C. Adequacy of the P_1 approximation equation

We assume that the time-domain Green's function solution of the P_1 equation adequately describes the transport of a photon in a turbid medium when the photon undergoes a sufficient number of collisions in its transit from the source to the detector. This means that the source/detector separation r should be sufficiently large such that $r \gg 1/(\mu_a + \mu_s)$ (or $r \gg 1/\mu_s$, since $\mu_s \gg \mu_a$), i.e., r is much greater than the mean-free path of a photon collision event. In these conditions, the transmitted light pulse is adequately described by the P_1 approximation in the time domain, and should thus also be adequately described by the P_1 approximation in the frequency domain at all modulation frequencies (the frequency-domain and time-domain expressions are related by the Fourier transformation). Once the source-detector separation is sufficiently large with respect to $1/\mu_s$, there is not an upper limit on the modulation frequencies at which the P_1 approximation equation is ade-

quate. Yoo, Liu, and Alfano have determined the minimum value of the product $r\mu_s'$ is of the order of 10 for adequate description of light pulse transport within the SDE [24]. Further studies are required to determine the minimum value of the product $r\mu_s$ for which light transport is adequately described within the P_1 approximation.

D. P_1 approximation equation versus the SDE

Figures 4–7 compare and contrast the predictions of the P_1 equation and the SDE in the frequency domain.

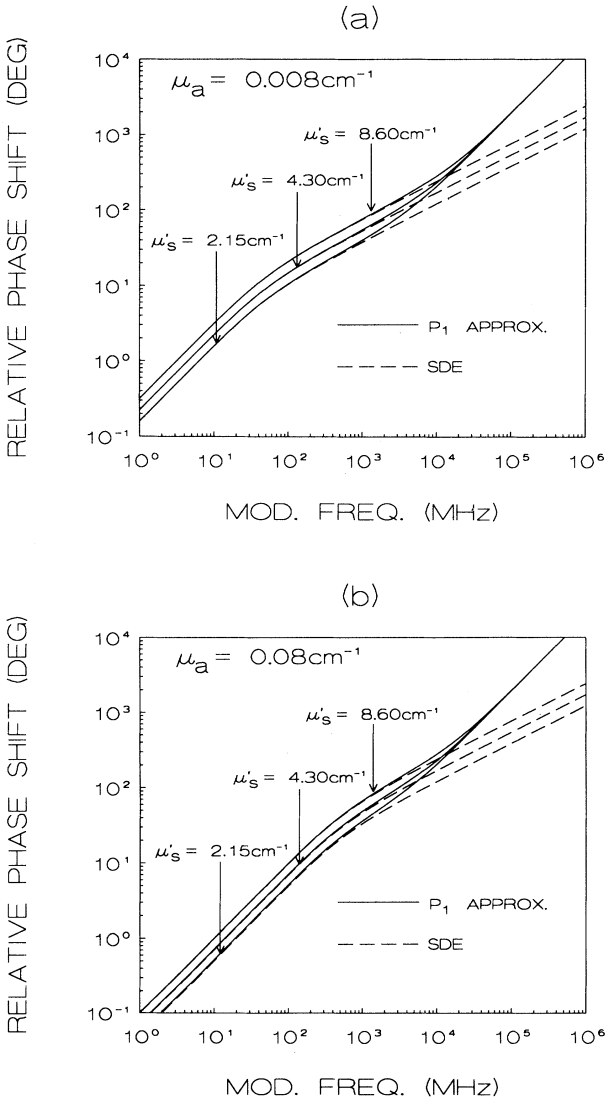

FIG. 4. (a) Relative phase shift vs modulation frequency. The solid curves were calculated from the P_1 approximation model [Eq. (13)], and the dashed curves were calculated from the standard diffusion equation (SDE) model. $r=1.8$ cm, $r_a=1.1$ cm, $c=2.26\times10^{10}$ cm/s, and $\mu_a=0.008$ cm^{-1}. (b) The same as (a), except that $\mu_a=0.08$ cm^{-1}.

In Figs. 4–7, $r=1.8$ cm, $r_0=1.1$ cm, and $c=2.26\times10^{10}$ cm/s. Figure 4 shows plots of relative phase shifts versus modulation frequency, calculated for three different reduced scattering coefficients and two different absorption coefficients with both the SDE expression given by Fishkin and Gratton [14] and the P_1 approximation expression [Eq. (13)]. Figure 5 is derived from Fig. 4 (as well as from one set of curves at $\mu_s'=25.80$ cm^{-1} not shown in Fig. 4). Figure 5 shows the difference in phase between the P_1 approximation model and the SDE model at four different reduced scattering coefficients and two different absorption coefficients for the medium. Since typical uncertainties in a measurement of Φ_{rel} are of the order of 0.2°, at modulation frequencies above 500 MHz we should be able to distinguish between the two models from a measurement of Φ_{rel} obtained from a medium with μ_s' and μ_a values within the range of values given in

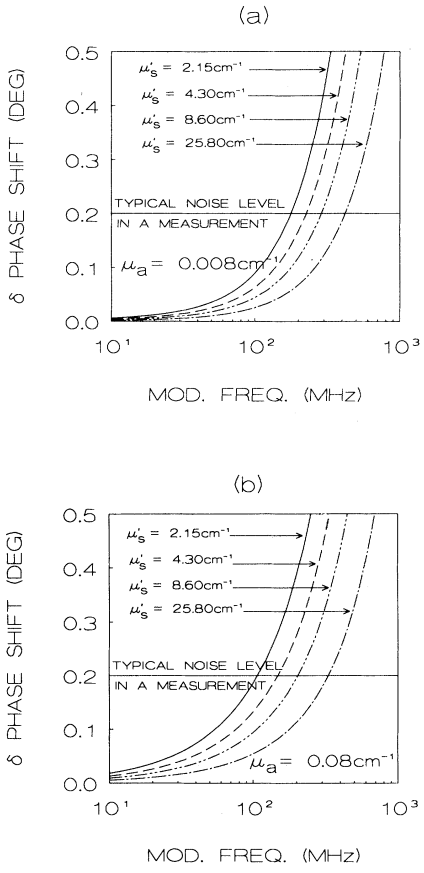

FIG. 5. (a) Phase-shift difference between the P_1 approximation model and the SDE model. These curves show the difference between the dashed and solid curves in Fig. 4 (and for one value of μ_s' not shown in Fig. 4, i.e., $\mu_s'=25.80$ cm^{-1}). $r=1.8$ cm, $r_0=1.1$ cm, $c=2.26\times10^{10}$ cm/s, and $\mu_a=0.008$ cm^{-1}. The horizontal line represents the typical noise level in a phase shift measurement, i.e., 0.2°. (b) The same as (a), except that $\mu_a=0.08$ cm^{-1}.

Fig. 4. Smaller values of μ_s' yield larger deviations between the two models at a given modulation frequency and μ_a value, as indicated by the curves in Fig. 5.

Figure 6 shows plots of relative demodulation versus modulation frequency, calculated for three different reduced scattering coefficients and two different absorption coefficients with both the SDE expression and P_1 approximation expression [Eqs. (11), (12), and (14)]. Figure 7 is derived from Fig. 6 (as well as from two sets of curves at $\mu_s'=17.20$ and 25.80 cm^{-1}, which are not shown in Fig. 6). Figure 7 shows the difference in demodulation between the P_1 approximation equation model and the SDE model at five different medium reduced scattering coefficients and two different absorption coefficients. Since typical uncertainties in a measurement of M_{rel} are of the order of 0.004, again, at modulation frequencies above 500 MHz we should be able to distinguish between the two models from a measurement of M_{rel} obtained from a medium with a μ_s' value within the range of values given in Fig. 6. Again, smaller values of μ_s' yield larger deviations between the two models at a given modulation frequency, as indicated by the curves in Fig. 7. Figure 7 also shows that, at sufficiently high values of μ_s', the description of M_{rel} data given by the P_1 approximation equation and the SDE at any modulation frequency should be the same. This is in contrast with the case of the phase shift. Figures 4 and 5 show that the difference between the phases predicted by the two models can be experimentally tested at any given μ_s', provided a high enough modulation frequency is reached.

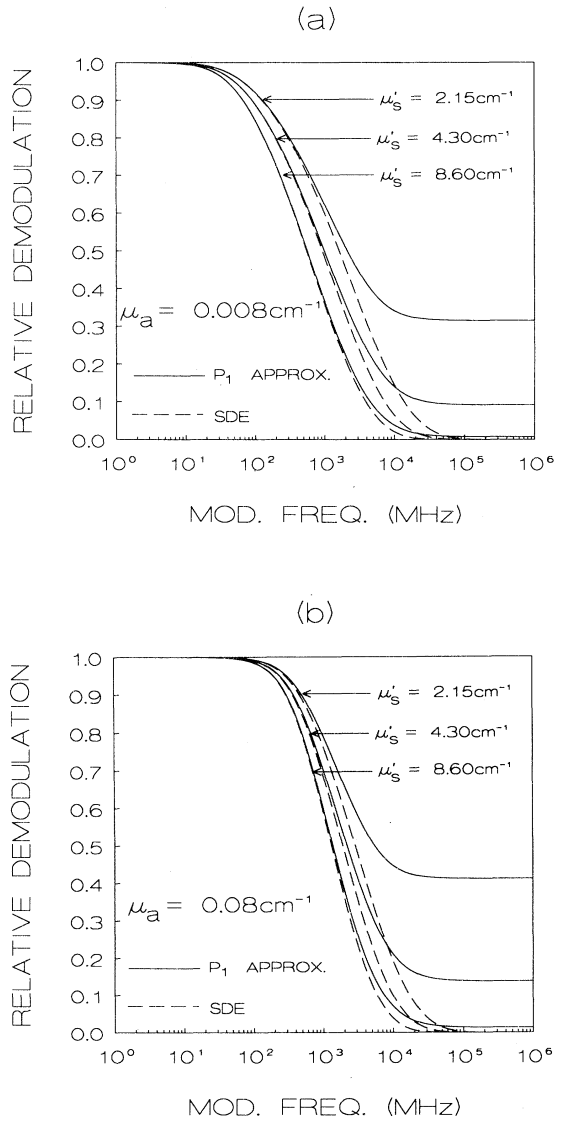

FIG. 6. (a) Relative demodulation vs modulation frequency. The solid curves are calculated from the P_1 approximation model [Eqs. (11), (12), and (14)], and the dashed curves are calculated from the SDE model. $r=1.8$ cm, $r_0=1.1$ cm, $c=2.26\times10^{10}$ cm/s, and $\mu_a=0.008$ cm^{-1}. (b) The same as (a), except that $\mu_a\pm0.08$ cm^{-1}.

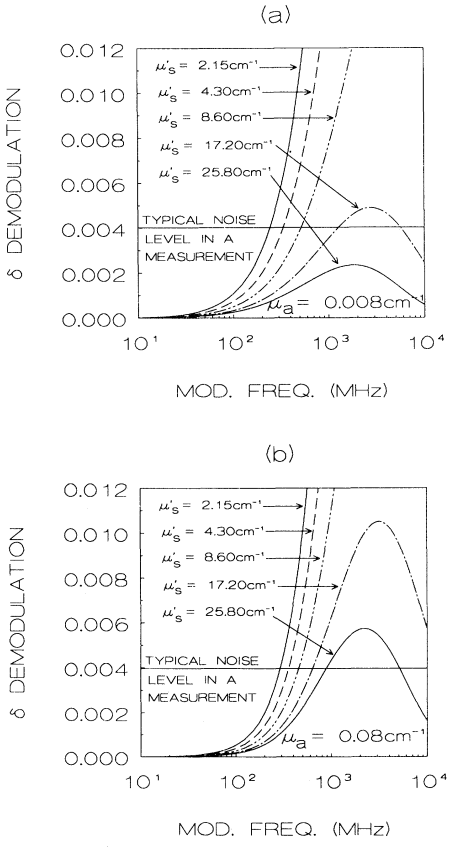

FIG. 7. (a) Demodulation difference between the P_1 approximation model and the SDE model. These curves show the difference between the dashed and solid curves in Fig. 6 (and for two values of μ_s' not shown in Fig. 6, i.e., $\mu_s'=17.20$ and 25.80 cm^{-1}). $r=1.8$ cm, $r_0=1.1$ cm, $c=2.26\times10^{10}$ cm/s, and $\mu_a=0.008$ cm^{-1}. The horizontal line represents the typical noise level in a demodulation measurement, i.e., 0.004. (b) The same as (a), except that $\mu_a=0.08$ cm^{-1}.

To experimentally study the deviations between the P_1 approximation equation and the SDE predictions, we used a superheterodyning microwave detection system to detect photon density waves generated in a turbid medium by a mode-locked laser. The superheterodyning technique that we employ extends the useful bandwidth of our microchannel plate detector to about 4 GHz (this frequency range is determined by the mixer–rf amplifier combination used in our instrument). We describe our frequency-domain instrument in detail in Sec. III.

III. EXPERIMENTAL APPARATUS AND METHOD

A. Description of the experimental apparatus

1. Laser system

A block diagram of the frequency-domain spectrophotometer is shown in Fig. 8. The light source used in our measurements is a mode-locked neodymium-yttrium-aluminum-garnet laser (Nd YAG, Coherent Antares 76-S, Santa Clara, CA) which produces a train of equally spaced light pulses with a repetition rate of 76.20 MHz and with its output frequency doubled to a wavelength of 532 nm. Each pulse is ~150 ps at full-width, half-maximum. Fourier analysis of the 76.20-MHz light pulse train yields a series of harmonic intensity-modulation frequencies with a spacing of 76.20 MHz between each harmonic [25]. A master oscillator is used as a reference for the frequency synthesizer that drives the neodymium-YAG laser mode locker. The same master oscillator is also used as an external reference for the microwave synthesizer (Hewlett-Packard, model 8341B), i.e., LOCAL OSCIL 1 in Fig. 8. A personal computer controls all instrument operations, which includes positioning of the ends of optical fibers F_s and F_d in the turbid medium.

The 76.20-MHz light pulse train (attenuated to ~50-mW average power) is split into two parts via a beam splitter, as shown in Fig. 8. One of the beams, which contains the majority of the power of the original beam, is focused via a lens onto optical fiber F_s, which conveys the laser light to the turbid medium under study. The other beam is directed onto a fast photodiode (35-ps rise time photodiode from Antel Optronics Inc., model AR-S2), which serves as the reference channel for our frequency-domain measurements [26,27]. The diameter of optical fiber F_s is 0.15 cm. The detector optical fiber (i.e., fiber F_d) consists of a 0.3-cm-diameter bundle of glass optical fibers, with a 0.1-cm aperture placed on the end of the fiber immersed in the turbid medium. The output of fiber F_d is directly in front of a 6-μm microchannel plate photomultiplier (MCP PMT) from Hamamatsu, model R2566U-01 [28].

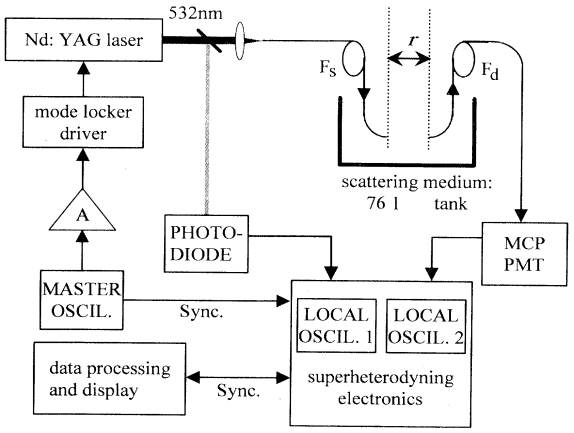

FIG. 8. Schematic of the superheterodyning, multifrequency, cross-correlation phase and modulation spectrophotometer used for measurements of the optical properties of turbid media. Light source: Coherent Antares 76-S mode-locked neodymium-yttrium-aluminum-garnet (Nd:YAG) solid state laser. The mode locker driver is from Coherent, model 7600. *A*, Hewlett-Packard 8447E Radio Frequency Amplifier. Detectors: (PHOTO-DIODE, 35-ps rise time photodiode from Antel Optronics Inc., model AR-S2; MCP PMT, 6-μm microchannel plate photomultiplier from Hamamatsu, model R2566U-01. OSCIL, radio frequency oscillators connected in a phase-locked loop to the data processing and display portion of the instrument. F_s, source optical fiber. F_d, detector optical fiber. A detailed schematic of the superheterodyning electronics is shown in Fig. 9.

2. Superheterodyning electronics

All modern frequency-domain instruments use the cross-correlation techniques introduced by Spencer and Weber [29]. The basic element of a frequency-domain instrument is the light source, which should have a power spectrum in the modulation frequency range of the instrument's operation. Using a narrow-pulsed, mode-locked laser, the power spectrum extends to about 50–100 GHz [30]. The light detector generally limits the bandwidth of a given instrument. Obtaining the maximum bandwidth from a given detector is a crucial point. For microchannel plate photomultiplier detectors (MCP PMT), the anode bandwidth is essentially the same as the cathode bandwidth, and the signal can be handled directly at the MCP PMT output [31].

The scheme of our electronic superheterodyning detection system is shown in Fig. 9. The output of the MCP PMT is separated into its ac and dc components. Special care is used in this part of the circuit. Since this is the only microwave frequency part of the signal processing, all components (capacitor, cables, connectors) must be rated for up to 4-GHz operation. We have verified, using a Hewlett-Packard spectrum analyzer (model 8569A), that the frequency response of this part of the circuit extends to about 4 GHz. After the microwave mixer *M*1 (Anzac, model MDC123), a frequency component of the signal is at low frequency (100 kHz). It can then be handled using standard electronic components. It should be noted that the average dc current from our MCP PMT must not exceed 200 nA, i.e., approximately 2 V after the dc current-to-voltage converter (again 10^7 V/A). About the same signal intensity with respect to the dc signal is

available at each one of the harmonic frequencies over a spectrum which extends up to the limit imposed by the detector. However, the ac part of the signal has a 50-Ω impedance due to the mixer input characteristics, which typically results in a 10-μV signal. These signal levels are very low, and a direct conversion to the 40-Hz region is difficult, since the ubiquitous 60-Hz line signal dominates. This difficulty is one of the reasons for using the intermediate conversion frequency, where amplification can be obtained in a low noise frequency region. The mixer has a conversion loss of about 7 dB (a factor of ~ 5), which reduces the signal output from the mixer to about 2 μV. The voltage level at the rf input of the mixer was fixed at about +10 dBm. This value was found to be optimal for the Anzac mixer. Some harmonics are produced at this high rf signal level, but we found that filtering of the second harmonic of the microwave frequency carrier is excellent and the linearity of the mixer output is also good. The mixer output is filtered using a 42IF301 ceramic IF filter transformer (Mouser Electronics, Mansfield, TX). This filter performs an impedance conversion from about 500 Ω to about 50 kΩ, providing a voltage gain of about a factor of 100. The output of the filter is then amplified by about a factor of 1000 and fed to the rf input of a second mixer (M2). The amplification

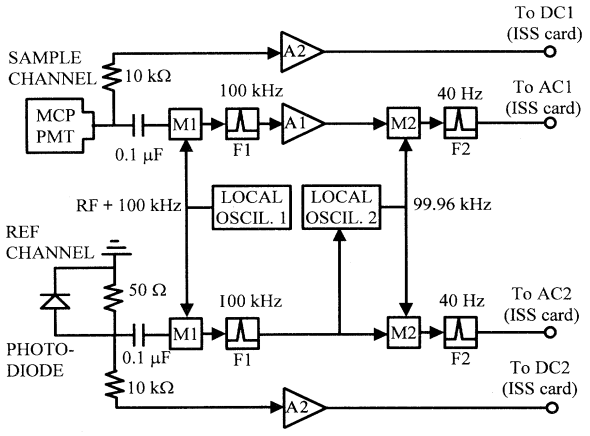

FIG. 9. Block diagram of the superheterodyning detection system. Detectors: MCP PMT, 6-μm microchannel plate photomultiplier from Hamamatsu, model R2566U-01; PHOTODIODE, 35-ps rise time photodiode from Antel Optronics Inc., model AR-S2. The radio frequency signals emitted from these detectors are split into ac and dc components. LOCAL OSCIL. 1, Hewlett-Packard 8341B Synthesized Sweeper, with a radio frequency output ranging over 10 MHz to 20 GHz. M1,2, double balanced mixers with their local oscillator input signals (RF+100 and 99.96 kHz, respectively), (RF, signal of a frequency matching that of the photon density wave under study). F1,2, narrow bandpass electronic filters for cross-correlation frequencies of 100 kHz and 40 Hz, respectively. *A*1, variable amplifier for ac signal. A2, dc amplifier LOCAL OSCIL. 2, tracking filter consisting of a phase detector, voltage controlled oscillator, and digital phase drifter.

of the signal at 100 kHz, second stage mixing, and further amplification and low pass filtering is obtained using a modified PAR, model 5204, lock-in amplifier, equipped with a tunable input filter set at 100 kHz. The low frequency filtering at 40 Hz and amplification is performed using standard electronics. The 99.96-kHz input of the second mixer is connected to the output of the tracking synthesizer, which provides a frequency exactly 40 Hz below the intermediate 100-kHz frequency. After bandpass filtering and amplification, the output of *M*2 contains all the information of the original high frequency signal. The reference channel operates in a similar fashion. The reference detector is a fast *p-i-n* photodiode (Antel Optronics Inc., model AR-S2) with 35-ps rise time [26,27]. A second, identical Anzac mixer performs the first frequency conversion to 100 kHz. The same kind of ceramic filter is used to isolate the 100-kHz component. Since the signal is relatively large, it is first split and one part is used as the reference frequency for the tracking synthesizer (i.e., LOCAL OSCIL. 2 in Figs. 8 and 9), the other is directly applied to the input of the second mixer where it is converted to 40 Hz.

At this point, four signals, corresponding to the ac and dc of the sample and reference, respectively, have been generated. These signals are applied to the inputs of an ISS A2D (ISS Inc., Champaign, IL) digital interface card for an IBM-PC computer, where the usual acquisition and processing is performed under computer control. The analog to digital card technology and digital processing with fast Fourier transform which process these signals is the current state of the art [32].

B. Measurement protocol in the turbid medium

The turbid medium under study was a macroscopically uniform 68-l mixture of a 1.3 skim milk to water ratio. The skim milk–water mixture was held in a 76 l glass tank of dimensions $60\times30\times42$ cm^3. The geometrical configuration of the detector optical fiber F_d with respect to the source optical fiber F_s was such that the aperture of fiber F_s directly opposed the aperture of fiber F_d in the turbid medium (Fig. 8). The ends of optical fibers F_s and F_d (with a maximum separation distance of 2.1 cm) were immersed in the multiply scattering medium as far as possible from the medium boundaries in order to best approximate the infinite medium boundary condition.

Frequency-domain measurements of phase shift Φ, and demodulation *M* were made at fourteen different intensity modulation frequencies (381.0, 457.2, 533.4, 762.0, 838.2, 914.4, 1143.0, 1371.6, 1524.0, 1905.0, 2057.4, 2438.4, 2819.4, and 3200.4 MHz) at source–detector separations ranging from 1.1 to 2.1 cm in 0.1-cm increments. The source-detector separation *r* was controlled by a motorized scanning device (Techno XYZ Positioning Table, New Hyde Park, NY), with the position reproducibility in *r* to within 10 μm). At a given modulation frequency $\omega/2\pi$, the phase shift Φ and demodulation *M* quantities measured at a distance *r* from the source were respectively compared to the Φ and *M* quantities measured at the $r_0 = 1.1$-cm source-detector separation. This enables us

to obtain the relative quantities Φ_{rel} and M_{rel}, defined in Eqs. (11)–(14). As noted by Fishkin *et al.* [6], the measurement of the relative demodulation and phase shift quantities (i.e., M_{rel} and Φ_{rel}) at a given value of $\omega/2\pi$ has the following advantage: terms which are dependent on the source emission properties are eliminated, as are the spectral response factors of the superheterodyning phase-sensitive detection system. When fitting our frequency-domain data (Φ_{rel} and M_{rel}) to Eqs. (13) and (14), respectively, to obtain the medium absorption and reduced scattering coefficients (μ_a and μ_s') at the light wavelength 532 nm, we assume that $n=1.33$ for the multiply scattering media under investigation (which is the index of refraction of water at the 532-nm wavelength considered). Typical instrumental uncertainties in our frequency-domain measurements are approximately 0.004 for M_{rel}, and 0.2° for Φ_{rel} [33].

IV. RESULTS

Figure 10 shows plots of the measured relative phase shift versus source-detector separation r in the 68-l 1:3 skim milk to water medium. All phase values were measured relative to the phase at the $r_0=1.1$ cm source-detector separation. For clarity, only four of the above mentioned modulation frequencies used in our experiments are shown in this plot. The solid lines are linear fits to these data. The linearity of the measured phase shifts with respect to r in Fig. 10 is consistent with the predictions of Eq. (13). Figure 11 shows plots of the natural logarithm of the measured relative demodulation versus r. As in Fig. 10, we only show four of the 14 modulation frequencies. The solid lines are linear fits to these data. The linearity of the data with respect to r at the three lowest modulation frequencies in Fig. 11 is consistent with the predictions of Eqs. (11), (12), and (14).

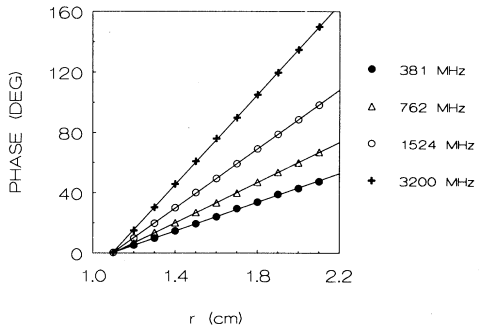

FIG. 10. Measured relative phase lag vs source/detector separation r, where the source and detector are immersed in a 68-l mixture of a 1:3 skim milk:water ratio. For clarity, we only show data acquired at four of the 14 modulation frequencies used in acquiring our data. The solid lines are linear fits to these data. The modulation frequencies at which we acquired our data ranged from 381.0 to 3200.4 MHz. The uncertainty in the data points is smaller than the size of the symbols representing the data.

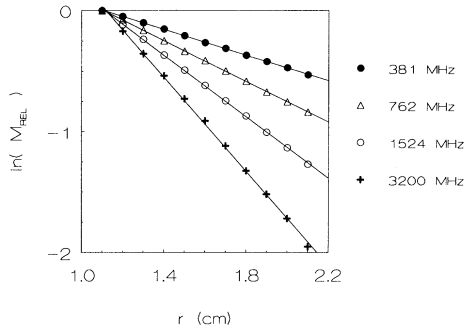

FIG. 11. Natural logarithm of the measured relative demodulation vs source/detector separation r, where the source and detector are immersed in a 68-l mixture of a 1:3 skim milk:water ratio. For clarity, we only show data acquired at four of the 14 modulation frequencies used in acquiring our data. The solid lines are linear fits to these data. The modulation frequencies at which we acquired our data ranged from 381.0 to 3200.4 MHz. The uncertainty in the data points is smaller than the size of the symbols representing the data.

The data acquired at 3200.4 MHz in Fig. 11 are not perfectly linear with respect to r. Rather, they show a slight downward curvature. This result is inconsistent with the predictions of both the P_1 approximation equation and the SDE.

Figures 12 and 13 show phase shift and demodulation data acquired in the 68-l 1:3 skim milk to water medium at $r=1.8$ cm relative to $r_0=1.1$ cm, at the 14 modulation frequencies. The solid curves in Figs. 12(a) and 13(a) represent fits to these data using the SDE expressions and the P_1 approximation equation expressions, respectively, for Φ_{rel} and M_{rel}. We emphasize that Φ_{rel} and M_{rel} were employed together to extract optical parameters μ_s' and μ_a from the plots of Figs. 12(a) and 13(a) (see Table I, where the correlated uncertainties given in this table were calculated using 0.98 probability limits for the confidence interval). These fits were obtained using the commercial package GLOBALS UNLIMITED (Laboratory for Fluorescence Dynamics, Dept. of Physics, University of Illinois at Urbana-Champaign) [34]. The residues of the SDE fit of Fig. 12(a) and the P_1 approximation equation fit of Fig. 13(a) are shown in Figs. 12(b) and 13(b), respectively. The residues of the SDE fit show strong systematic trends, and most of these residues are beyond the range of uncertainty of our measurements (i.e., $\Delta\Phi_{rel}=\pm 0.2°$ and $\Delta M_{rel}=\pm 0.004$). This indicates that the SDE does not provide an accurate description of the data over the range of modulation frequencies studied. The residues of the P_1 approximation equation fit show much less of a systematic trend, and are for the most part within the range of uncertainty of our measurements.

To further verify the relative accuracy of the P_1 approximation equation as compared with the SDE, we have also extracted the optical parameters μ_s' and μ_a

TABLE I. Optical parameters of the 68-l 1:3 skim milk:water solution obtained by fitting the frequency-domain data obtained from this medium to the P_1 equations and the SDE. All of the data fits were performed using 0.98 probability limits for the confidence interval. Table I is organized in the following manner: a row contains the optical parameters obtained from a particular combination of phase and/or demodulation data used in the calculation of the χ^2 surface; a column contains an optical parameter calculated from a given frequency-domain model for light transport in turbid media (i.e., either the P_1 model or the SDE).

	P_1 approximation fit		SDE fit	
	μ_s' (cm^{-1})	μ_a (cm^{-1})	μ_s' (cm^{-1})	μ_a (cm^{-1})
Phase & Demodulation Fit	4.26±0.13	0.0076±0.0034	4.95±0.30	0.017±0.013
Phase Fit Only	4.19±0.07	0 to 0.0038	5.06±0.37	0.026±0.025
Demodulation Fit Only	4.34±0.34	0.0086±0.0027	3.35±0.41	0.0046±0.0031

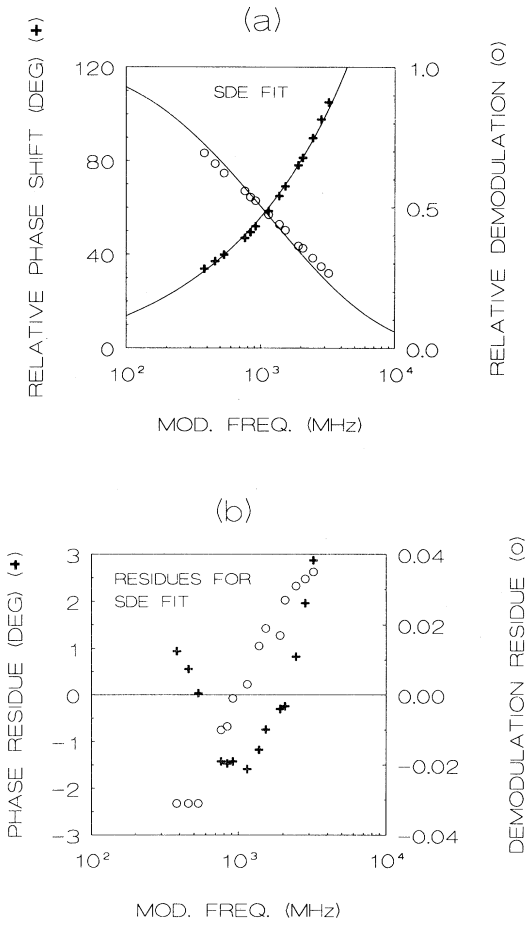

FIG. 12. (a) Phase and demodulation data acquired at $r=1.8$ cm relative to $r_0=1.1$ cm. The solid curves represent a fit to these data using the standard diffusion equation (SDE) expressions for the relative phase shift and the relative demodulation. Assuming that $c=2.26\times10^{10}$ cm/s, the values for the reduced scattering and absorption coefficients obtained from this fit are shown in Table I. (b) Residues of the SDE fit to the data shown in (a). The uncertainty in the data points is smaller than the symbols representing the data.

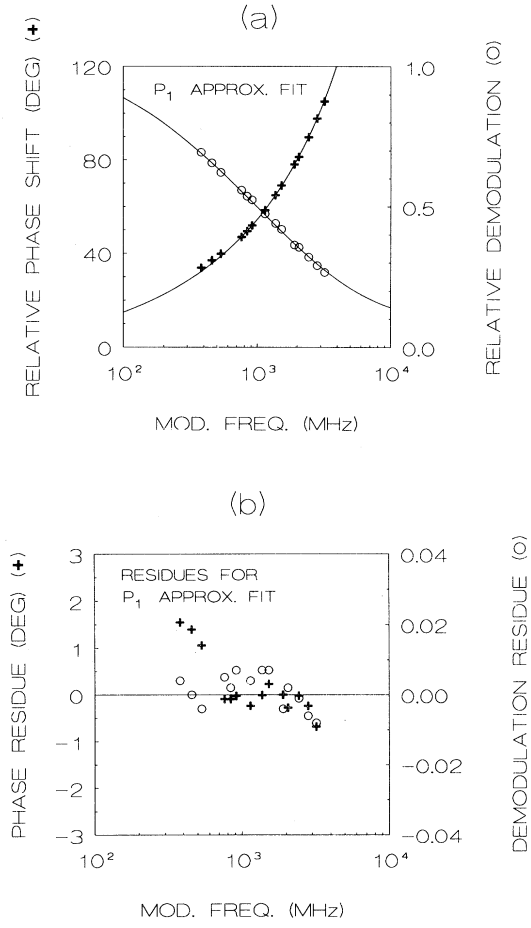

FIG. 13. (a) Phase and demodulation data acquired at $r=1.8$ cm relative to $r_0=1.1$ cm. The solid curves represent a fit to these data using the P_1 approximation equation expressions for the relative phase shift and the relative demodulation. Assuming that $c=2.26\times10^{10}$ cm/s, the values for the reduced scattering and absorption coefficients obtained from this fit are shown in Table I. (b) Residues of the P_1 approximation fit to the data shown in (a). The uncertainty in the data points is smaller than the symbols representing the data.

from the phase data only and the demodulation data only. The results of these fits using both the P_1 approximation equation and the SDE are shown in Table I. The μ_s' and μ_a values extracted from the P_1 approximation equation fits to the data are more consistent than the μ_s' and μ_a values extracted from the SDE fits to the data (see Table I). The fitted parameter μ_s' is relatively uncorrelated with the fitted parameter μ_a in all of the P_1 approximation fits to our data. The μ_s' and μ_a values obtained from the SDE fits to our data are more correlated than those obtained from the P_1 approximation equation fits. The value of μ_a at the optical wavelength of 532 nm extracted from the P_1 approximation fits to data obtained in our skim milk–water mixture (i.e., $\mu_a = 0.0076 \pm 0.0034$ cm^{-1}, from the relative phase shift and demodulation data) is the same value for μ_a that Fishkin *et al.* [6] obtained for a liposyn-water mixture at 532 nm. This coincidence may imply that only water absorbs at this wavelength.

The χ^2 surface calculated only from the P_1 expression for the phase [Eq. (13)] over the frequency range of 381.0 MHz–3.2 GHz is relatively flat with respect to the parameter μ_a, with the χ^2 surface at a minimum for $\mu_a \approx 0$ cm^{-1}. The values for μ_a which fall within the 0.98 probability limits for the confidence interval of the phase fit range from 0 to 0.0038 cm^{-1} (see Table I). (We have required that a fit always yield positive values for μ_s' and μ_a). We have explored the χ^2 surface calculated only from the relative phase shift [Eq. (13)] over different modulation frequency ranges in order to determine if there is an optimal range of modulation frequencies from which μ_a can be determined using phase data only. By inspection of the χ^2 surface for the P_1 approximation using only the phase in the range 381 MHz–10 GHz, we concluded that when the parameter μ_a is of the order of 0.01 cm^{-1}, it may be scarcely determined. However, acquisition of phase only data over the range 20–500 MHz dramatically increases the accuracy with which μ_a may be determined when it is of the order of 0.01 cm^{-1} (recall that our data set extends over the range 381 MHz–3.2 GHz). This result is not surprising if one examines Fig. 4, which shows lots of relative phase shift versus modulation frequency. In Fig. 4(a), μ_a is of the order of 0.01 cm^{-1}. The maximum curvature in the phase shift with respect to modulation frequency in Fig. 4(a) occurs roughly between 20 and 500 MHz, whereas the phase shift in this figure is relatively linear at modulation frequencies greater than 500 MHz and at modulation frequencies less than 20 MHz. In Fig. 4(b), μ_a is of the order of 0.1 cm^{-1}. The maximum curvature in the phase shift with respect to modulation frequency in Fig. 4(b) occurs roughly between 200 MHz and 5 GHz. An order of magnitude increase in medium absorption μ_a thus seems to increase by an order of magnitude the optimal modulation frequency range for determining μ_a from phase only data. This result indicates that if one is to use the phase shift only to determine the optical parameter μ_a, the range of modulation frequencies used must be carefully chosen so as to include the region of maximum curvature of the phase shift with respect to modulation frequency in the calculation of the χ^2 surface. This result is consistent with the conclusions of Tromberg *et al.* [3], who used the SDE expression for the phase to recover μ_a and μ_s' from phase only data.

V. CONCLUSION

We have shown that the difference between the SDE [i.e., Eq. (5)] and the more complete P_1 approximation to the Boltzmann transport equation [i.e., Eq. (1)] is significant only at modulation frequencies of several hundred MHz or greater. The modulation frequency at which the two models begin to significantly differ is dependent on the reduced scattering coefficient of the medium μ_s'. The point of significant difference is determined by the typical noise levels in a frequency-domain measurement (see Figs. 5 and 7). Smaller values of μ_s' yield larger deviations between the two models at a given modulation frequency. Figure 1(b) shows an $r\mu_s'$ versus $r\omega/2\pi$ diagram of the regions of validity of the SDE and P_1 approximations. At higher modulation frequencies and relatively small reduced scattering coefficients, the P_1 approximation should be used for the description of the propagation of light in turbid media. However, for relatively large reduced scattering coefficients and/or low frequencies, the SDE approximation can be adequate for the description of light propagation in turbid media. We note that at very small values of the scattering coefficient, neither approximation is adequate and higher order approximations to the Boltzmann transport equation may be required to describe photon migration in the lower scattering regime adequately. It is also important to realize, as shown in Fig. 1(b), that the distance between the source and detector is another important factor for the applicability of the P_1 approximation. The smaller the scattering coefficient, the larger the source-detector separation should be for the applicability of the P_1 approximation.

The frequency-domain P_1 approximation equation predicts that as the modulation frequency approaches infinity, the phase velocity of the photon density wave V_p asymptotically approaches $c/\sqrt{3}$ (see Fig. 2). We have plotted the Fourier transform of our frequency-domain solution to the P_1 approximation equation in Fig. 3 using the same optical parameters that generated Fig. 2. The time-domain results we obtained when we Fourier transformed our frequency-domain Green's function [i.e., the frequency-dependent part of Eq. (7)] are identical to the results that Kaltenbach and Kaschke calculated directly from their analytical time-domain Green's function [22]. Examination of these time-domain calculations shows that at a distance r from the light source, the earliest arriving photons generated by the pulsed source $S^{(0)}(\mathbf{r},t)=\delta(\mathbf{r})\delta(t)$ arrive at a time $t_{\min}=r/(c/\sqrt{3})$ according to the P_1 approximation equation. This result contradicts previous claims [19–21] that the P_1 approximation to the Boltzmann transport equation predicts that a light pulse propagates with an average speed of $c/\sqrt{3}$ in a thick, turbid medium.

Examination of the P_1 approximation equation fits and

the SDE fits to our frequency-domain data (see Figs. 12 and 13, and Table I) indicates that the P_1 approximation equation gives a more accurate and self consistent description of our data than the SDE. However, there is still a systematic trend in the residues obtained from the P_1 approximation equation fits, which may indicate that the P_1 approximation equation does not provide a complete description of our data. Boas *et al.* [35] have derived higher order frequency-domain P_3 *approximation* expressions which may provide a better representation of our observations than the P_3 approximation expressions. The conditions for the applicability of higher order approximations to the Boltzmann transport equation for describing photon migration in turbid media is an important problem which may be of use to the community of researchers who use diffusing light to image turbid media. In this paper, we have studied the physical meaning of the P_1 approximation. The mathematical limit of the higher order P_L approximations to the Boltzmann transport equation has been established, but the physical picture of the process described by the addition of higher order terms has not been investigated, as yet. In any case, our studies of the χ^2 surface calculated from the phase only indicate that choosing an appropriate modulation frequency range is critical for extracting an accurate value of the absorption of the medium. The range of absorption coefficients that can be well determined by a measurement of the phase scales with the modulation frequency range utilized: the larger the absorption coefficient, the higher the optimal modulation frequency range for determining the absorption coefficient of the medium.

ACKNOWLEDGMENTS

These experiments and analyses of the data produced were performed at the Laboratory for Fluorescence Dynamics (LFD) in the Department of Physics at the University of Illinois at Urbana-Champaign (UIUC). The LFD and this work is supported by the National Institutes of Health (RR03155 and CA57032) and by UIUC. The authors thank F. Prendergast for providing the microwave electronics for this project, and J. Beechem, J. Sutin, and G. Perez for their help. The authors also thank R. Haskell, L. Svaasand, and B. Tromberg, who gave us the idea to create Fig. 2 of this work.

[1] E. Gratton, W. W. Mantulin, M. J. vandeVen, J. B. Fishkin, M. B. Maris, and B. Chance, in *Proceedings of the Third International Conference on Peace through Mind/Brain Science,* edited by Hamamatsu Photonics (Hamamatsu, Hamamatsu City, Japan, 1990), p. 183.

[2] M. S. Patterson, J. D. Moulton, B. C. Wilson, K. W. Berndt, and J. R. Lakowicz, Appl. Opt. **30**, 4474 (1991).

[3] B. J. Tromberg, L. O. Svaasand, T. Tsay, and R. C. Haskell, Appl. Opt. **32**, 607 (1993).

[4] S. J. Madsen, E. R. Anderson, R. C. Haskell, and B. J. Tromberg, Opt. Lett. **19**, 1934 (1994).

[5] S. Fantini, M. A. Franceschini, J. B. Fishkin, B. Barbieri, and E. Gratton, Appl. Opt. **33**, 5204 (1994).

[6] J. B. Fishkin, P. T. C. So, A. E. Cerussi, S. Fantini, M. A. Franceschini, and E. Gratton, Appl. Opt. **34**, 1143 (1995).

[7] K. M. Case and P. F. Zweifel, *Linear Transport Theory* (Addison-Wesley, Reading, MA, 1967), Chap. 8, pp. 196–199.

[8] J. J. Duderstadt and W. R. Martin, *Transport Theory* (Wiley, New York, 1979), Chap. 4, pp. 219–221.

[9] M. A. O'Leary, D. A. Boas, B. Chance, and A. G. Yodh, Phys. Rev. Lett. **69**, 2658 (1992).

[10] D. A. Boas, M. A. O'Leary, B. Chance, and A. G. Yodh, Phys. Rev. B **47**, R2999 (1993).

[11] I. V. Yaroslavsky, H. J. Schwarzmaier, A. N. Yaroslavsky, and V. V. Tuchin, in *Photon Transport in Highly Scattering Tissue,* edited by S. Avrillier, B. Chance, G. J. Müller, A. V. Priezzhev, and V. V. Tuchin [Proc. Soc. Photo-Opt. Instrum. Eng. **2326**, 465 (1995)].

[12] R. C. Haskell, L. O. Svaasand, S. J. Madsen, F. E. Rojas, T. C. Feng, and B. J. Tromberg, Proc. Soc. Photo-Opt. Instrum. Eng. **2389**, 284 (1995).

[13] S. Fantini, M. A. Franceschini, S. A. Walker, J. S. Maier, and E. Gratton, Proc. Soc. Photo-Opt. Instrum. Eng. **2389**, 340 (1995).

[14] J. B. Fishkin and E. Gratton, J. Opt. Soc. Am. A **10**, 127 (1993).

[15] E. Gratton, W. W. Mantulin, M. J. vandeVen, and J. B. Fishkin, Bioimaging **1**, 40 (1993).

[16] P. Krämmer, H. Bartelt, H. Fischer, and B. Schmauss, Proc. Soc. Photo-Opt. Instrum. Eng. **2326**, 65 (1995).

[17] K. Furutsu and Y. Yamada, Phys. Rev. E **50**, 3634 (1994).

[18] W. F. Cheong, S. A. Prahl, and A. J. Welch, IEEE J. Quantum Electron. **26**, 2166 (1990).

[19] A. Ishimaru, Appl. Opt. **28**, 2210 (1989).

[20] K. Shimizu and A. Ishimaru, Opt. Lett. **5**, 205 (1980).

[21] A. Ishimaru, J. Opt. Soc. Am. **68**, 1045 (1978).

[22] J. Kaltenbach and M. Kaschke, in *Medical Optical Tomography: Functional Imaging and Monitoring,* edited by G. Müller (SPIE, Washington, DC, 1993), p. 65.

[23] G. Zaccanti, P. Bruscaglioni, A. Ismaelli, L. Carraresi, M. Gurioli, and Q. Wei, Appl. Opt. **31**, 2141 (1992).

[24] K. M. Yoo, Feng Liu, and R. R. Alfano, Phys. Rev. Lett. **64**, 2647 (1990).

[25] J. R. Alcala, E. Gratton, and D. M. Jameson, Anal. Inst. **14**, 225 (1985).

[26] Antel Optronics, Inc. Model AR-S2 Picosecond Photodetector Manual (1988) (unpublished).

[27] Antel Optronics, Inc. Technical Data SHeet 201A (1988) (unpublished).

[28] Hamamatsu Technical Data Wide frequency response MCP-PMT, R2566U (Feb. 1989) (unpublished).

[29] R. Spencer and G. Weber, Ann. N.Y. Acad. Sci. **158**, 361 (1969).

[30] E. Gratton and R. Lopez-Delgado, Rev. Sci. Instrum. **50**, 789 (1979).

[31] J. R. Lakowicz, G. Laczko, and I. Gryczynski, Rev. Sci. Instrum. **57**, 2499 (1986).

[32] B. A. Feddersen, D. W. Piston, and E. Gratton, Rev. Sci. Instrum. **60**, 2929 (1989).

[33] B. Barbieri, F. De Piccoli, M. J. vandeVen, and E. Gratton, in *Time Resolved Laser Spectroscopy in Biochemistry*

II, edited by J. R. Lakowicz [Proc. Soc. Photo-Opt. Instrum. Eng. **1204**, 158 (1990)].

[34] J. M. Beechem and E. Gratton, in *Time Resolved Laser Spectroscopy in Biochemistry,* edited by J. R. Lakowicz [Proc. Soc. Photo-Opt. Instrum. Eng. **909**, 70 (1988)].

[35] D. A. Boas, H. Liu, M. A. O'Leary, B. Chance, and A. G. Yodh [Proc. Soc. Photo-Opt. Instrum. Eng. **2389**, 240 (1995)].